Journal of Power Sources 463 (2020) 228205

Contents lists available at ScienceDirect

Journal of Power Sources

journal homepage: www.elsevier.com/locate/jpowsour

Fabrication strategies for high-rate TiO_2 nanotube anodes for Li ion energy storage

Yu Jiang [a,*], Charles Hall [a], Patrick A. Burr [b], Ning Song [a], Derwin Lau [a], Jodie Yuwono [a], Da-Wei Wang [c], Zi Ouyang [a], Alison Lennon [a]

[a] School of Photovoltaic and Renewable Energy Engineering, UNSW, Sydney, NSW, 2052, Australia
[b] School of Mechanical and Manufacturing Engineering, UNSW, Sydney, NSW, 2052, Australia
[c] Particles and Catalysis Research Group, School of Chemical Engineering, UNSW, Sydney, NSW, 2052, Australia

HIGHLIGHTS

- Three fabrication strategies for TiO_2 NT electrodes have been investigated.
- Current collector geometry, crystal structure of TiO_2 and NT geometry were studied.
- 3D Ti foams enable higher mass loading, shorter NTs and enhanced NT adhesion.
- Amorphous TiO_2 electrodes show superior rate performance than anatase.
- Achieved high capacity (507 uAh cm^{-2} at 50 μA cm^{-2}), rate and stable 2000 cycles.

ARTICLE INFO

Keywords:
High rate Li ion battery
TiO_2 nanotubes
Amorphous TiO_2
Nanotube geometry
3D metal current collectors

ABSTRACT

Fabrication strategies for TiO_2 nanotube (NT) electrodes were optimised with an aim to improve the understanding of the material attributes required for enhanced areal capacity without compromising rate capability and cycling stability in these alternative high-rate anodes for Li ion batteries. The investigation considered the effects of: i) the geometry of the current collecting scaffolds (planar or foam); ii) crystallographic structure of TiO_2 (amorphous or crystalline); and iii) NT geometry arising from use of different anodisation conditions. By optimising the three strategies concurrently, we were able to demonstrate amorphous TiO_2 NT electrodes on a Ti foam current collector with not only a high areal capacity of 507 μAh cm^{-2} (recorded at 50 μA cm^{-2}) but also improved rate capability (retained a capacity of 347 μAh cm^{-2} at 5 mA cm^{-2}) and long-term cycling stability (capacity retention of 83% after 2000 cycles). This achievement of high areal capacity, rate capacity and cycling stability, which is superior to that reported previously, is attributed to the combined higher surface area of the foams, faster Li ion diffusion in the amorphous TiO_2 compared to crystalline TiO_2 and improved electronic conductivity and structural stability of the NTs enabled by limiting NT lengths.

1. Introduction

High rate capability and long cycle life are becoming increasingly important for lithium ion batteries (LIBs) to meet the future requirements for electric vehicles and renewable energy integration [1–3]. Commercially available LIBs typically use graphite as the anode material, however the low lithiation potential of graphite (~0.1 V vs. Li/Li^+) has posed several challenges for this anode material to be used in high-rate LIBs. First, a thick layer of solid electrolyte interface (SEI) is formed at the graphite surface due to decomposition of electrolyte species at low potentials [4–6]. Although this layer still permits the transport of Li ions upon battery cycling, it electronically passivates the graphite surface partially restricting ionic transport and limiting charging and discharging rates of the LIB. Second, at high rates, the continued growth of this SEI during battery cycling results in increased impedance, electrolyte depletion and reduced battery cycle life [7–9]. Finally and perhaps most importantly from a safety perspective, Li dendrites can form at the graphite anode surface when it is lithiated at high rates and cause short circuits leading to thermal runaway and fires [10,11].

* Corresponding author. TETB Building Reception, UNSW, Sydney, NSW, 2052, Australia.
E-mail address: yu.jiang1@unsw.edu.au (Y. Jiang).

https://doi.org/10.1016/j.jpowsour.2020.228205
Received 18 November 2019; Received in revised form 30 March 2020; Accepted 15 April 2020
Available online 27 April 2020
0378-7753/

Various TiO_2 polymorphs have frequently been proposed as alternative anode materials for high-rate LIBs due to their small volume change (<4%) upon Li ion insertion/extraction [12] and higher lithiation potentials (~1.5–1.7 vs. Li/Li^+) [13,14]. The latter attribute diminishes the risk of Li plating and dendrite formation, especially when a battery is cycled at high rates [14,15]. Additionally, although also affected by other factors [4], electrolyte decomposition is typically lessened at higher lithiation cut-off potentials and this reduces SEI formation [16] hence lowering the battery impedance on charging and discharging. However, bulk TiO_2 suffers from low electronic and ionic conductivity [17,18] which inherently limits its rate performance. One approach to overcome these limitations is to nanostructure TiO_2 to provide shorter diffusion paths for both electrons and ions and to increase the electrode/electrolyte interface area for greater reactivity. Numerous TiO_2 nanostructures have been successfully synthesised, including nanoparticles [19–24], nanotubes [25–34], nanowires [35,36] and mesoporous structures [37,38], with considerable improvements in storage capacities and rate capabilities being achieved. Of particular interest have been the self-organised and electrochemically grown TiO_2 nanotubes (NTs) due to their fabrication simplicity, large electrode/electrolyte interface area, nanoscale diffusion pathways via tube walls and self-supported structure, which eliminates the need for binders and conductive additives [29,39–41].

Various aspects of TiO_2 NT electrodes have been investigated and their effect on Li ion storage properties of the electrodes has been reported. In most studies, the TiO_2 NT electrodes have been prepared by electrochemically anodising planar Ti foils, with the foils being utilised as current collecting scaffolds. However, Bi et al. [42] and Choi et al. [43] explored the use of three-dimensional (3D) porous Ti foams as higher surface area current collectors for NT electrodes. Although improved areal capacities and rates were achieved compared to TiO_2 NT electrodes prepared using foils, the reported capacities at high rates (83 μAh cm^{-2} at 0.5 mA cm^{-2} [42] and 335 μAh cm^{-2} at 2.9 mA cm^{-2} [43], respectively) and cyclability (<100 cycles) were still limited. Several studies have investigated the influence of anodisation parameters on the geometries of NTs formed on planar foils and their effects on the Li ion storage properties of these electrodes [29,32,41,44]; however, the influence of these parameters on NT electrodes prepared using porous foams is not well understood as the porous foam geometry can affect both NT formation and electrolyte access due to the presence of tortuous paths in the foam. Furthermore, to increase the complexity of any optimisations of NT formation and cycling, the crystallographic structure of the TiO_2 in the NTs can also significantly affect the electrochemical properties of the electrodes [39,45–47].

Consequently, despite numerous developments in TiO_2 NT electrodes for high-rate LIBs, achievement of high areal capacity and rate performance whilst retaining excellent long-term cycling stability has remained challenging. In this paper, we systematically investigated three electrode fabrication strategies with an aim to improve the understanding of the material attributes required for enhanced areal capacity, rate capability and cycle life in TiO_2 NT electrodes. The first section reports on the use of planar foils and 3D porous foams as current collecting scaffolds for TiO_2 NT electrodes and compares the geometric and electrochemical properties of NTs grown on the foil and foam, respectively. Then, a comparison between amorphous (a-TiO_2) and anatase (c-TiO_2) NTs electrodes is reported to elucidate the impact of the crystallographic structure of TiO_2 NTs on the Li ion storage properties of these electrodes. The third section reports on the influence of anodisation voltage, anodisation duration and NH_4F concentration on the morphology of TiO_2 NTs grown on Ti foams and how this impacts the capacity and rate capability of the electrodes. Finally, the electrochemical performance of the NTs electrodes fabricated from this study was compared to that of previously reported comparative electrodes. This study demonstrates that TiO_2 NT electrodes fabricated using a facile and scalable one-step anodisation process can achieve excellent areal capacities, rate capability and long-term cyclability over 2000 cycles through a careful and concurrent optimisation strategy.

2. Experimental

2.1. Electrode preparation

TiO_2 NT electrodes were prepared electrochemically using a one-step anodisation process. Before anodisation, the commercially pure Ti foils and foams (>99.9% Ti, obtained from TOB New Energy) were cleaned by ultrasonication in acetone, isopropyl alcohol and deionised water for 10 min each. The foams were then immersed in the anodisation electrolyte in a vacuum environment for 40 min to ensure that the electrolyte accessed the inner surface of the foams. Anodisation was performed in a two-electrode configuration with the Ti foam as the anode and a platinised Ti plate as the cathode. TiO_2 NTs were grown by applying a constant voltage to the Ti substrates after a voltage ramp from 0 V to the designated voltage. The voltage was supplied by an IviumStat.XRe potentiostat (Ivium Technologies). After anodisation, the Ti foams and foils were first rinsed in deionised H_2O, then soaked sequentially in 20, 40, 80 vol% ethanol and deionised H_2O mixtures, and pure ethanol for 5 min each. Finally, the rinsed TiO_2 NTs electrodes were dried in air.

In Section 3.1, the Ti foams and foils were anodised in a glycerol electrolyte comprising 0.45 M NH_4F (Sigma-Aldrich) and 2.5 vol% deionised H_2O with an anodisation voltage of 35 V for 50 min. In Section 3.2, a-TiO_2 NT electrodes were prepared by anodising Ti foams in a glycerol electrolyte comprising 0.45 M NH_4F and 2.5 vol% deionised H_2O with an anodisation voltage of 35 V for 50 min. To prepare c-TiO_2 electrodes, the as-anodised TiO_2 NTs were annealed at 400 °C for 1 h in air. In Section 3.3, the TiO_2 NT electrodes were prepared by anodising Ti foams using the anodisation parameters as shown in Table 1.

2.2. Material characterisation

Scanning electron microscope (SEM) and transmission electron microscope (TEM) images were acquired by an FEI Nova NanoSEM 450 FE-SEM microscope and a Phillips CM200 TEM microscope, respectively. Selected area electron diffraction (SAED) patterns were obtained to verify the crystallinity of the TiO_2 NTs using an FEI Tecnai G2 20 TEM microscope with an aperture diameter of ~200 nm. The composition of the NTs was investigated using X-ray photoelectron spectroscopy (XPS) using a Thermo Scientific UK ESCALAB250Xi system under an ultra-high vacuum. The X-ray source was monochromated Al K_α (energy of 1486.68 eV) with the binding energy scale being calibrated using a carbon reference (C 1s = 284.8 eV). Ex-situ thin-film X-ray diffraction

Table 1
Summary of anodisation parameters used in the experiments reported in Section 3.3.

Investigation Parameter	NH_4F Concentration (mol l^{-1})	Anodisation Voltage (V)	Anodisation Duration (min)
NH_4F Concentration	0.075	50.0	50.0
	0.150	50.0	50.0
	0.300	50.0	50.0
	0.375	50.0	50.0
	0.450	50.0	50.0
Voltage	0.450	12.5	50.0
	0.450	20.0	50.0
	0.450	27.5	50.0
	0.450	35.0	50.0
	0.450	40.0	50.0
Duration	0.450	35.0	8.33
	0.450	35.0	16.7
	0.450	35.0	50.0
	0.450	35.0	100
	0.450	35.0	200
	0.450	35.0	300

(XRD) was conducted in a PANalytical Empyrean diffractometer with Cu K_α emission ($\lambda = 1.5418$ Å). Raman spectroscopy was recorded using a Renishaw inVia spectrometer with a laser wavelength of 532 nm.

2.3. Electrochemical characterisation

TiO_2 NT electrodes were cut into 1 cm^2 square and coupled with Li foils (0.25 mm thick and 99% purity) and assembled into R2025-type coin cells for electrochemical characterisation. Prior to cell assembly, prepared TiO_2 NT electrodes were dried in a vacuum oven at 60° for 24 h to remove any residual solvent. The TiO_2 NT film on the rear surface of the foam/foil was scratched off to ensure a good electrical contact to the metal of the coin cell. A volume of 80 μL of 1 M $LiPF_6$ in a 1:1 v/v mixture of ethylene carbonate (EC) and ethyl methyl carbonate (EMC) (Sigma Aldrich) was used as the electrolyte and battery-grade microporous membranes (Celgard® 2325, 25 μm thick) as separators. All coin cells were assembled in an Ar-filled glovebox (MBRAUN MB-LABStar 1250/780) with H_2O and O_2 content maintained < 0.5 ppm. Galvanostatic charge and discharge (GCD) measurements were performed using either a Neware BTS4000 battery testing system or an Ivium-n-Stat with sModule 2 A/20 V potentiostat (Ivium Technologies). Battery charging and discharging were measured for a potential range of 1.0–3.0 V with respect to the Li/Li^+ potential and these data were used to estimate the electrode areal capacities at various current densities. Cyclic voltammetry (CV) measurements were performed using Ivium-n-Stat with sModule 2 A/20 V potentiostat (Ivium Technologies) for a potential range of 1.0–3.0 V with respect to the Li/Li^+ potential. For the scan-rate-dependent CV analysis, the *b*-values were determined from the anodic peak current I_p in CV curves at various voltage scan rates v according to Refs. [20,48,49]:

$$I_p = av^b \tag{2.1}$$

For the rate performance comparison of the TiO_2 NT electrodes in Section 3.3, the rate parameter, *R*, was used rather than the current density (in mA cm^{-2}) or C-rate as *R* represents the time required to charge and discharge an electrode or battery and therefore is a more useful rate metric for practical battery use cases. Also calculations of *R* make no assumptions of the theoretical capacity of the electroactive material. The rate parameter *R* is defined by Refs. [50,51]:

$$R = \frac{I/A}{(Q/A)_{exp}} \tag{2.2}$$

where I/A is the charge and discharge areal current and $(Q/A)_{exp}$ is the experimentally measured areal capacity of the electrodes at the corresponding current.

3. Results and discussion

3.1. Foam vs. foil current collectors

The 3D Ti foams provided a percolating metallic network for electron transport and microscale pores for ion diffusion pathways to the electroactive material surface (see Fig. 1a). An X-ray computed tomography analysis of the foam revealed that the foams used in this study were ~600 μm thick and had an open surface area (i.e., the surface area accessible to electrolyte) of ~14.6 mm^2 per mm^3 and a porosity of ~25% (further details of the foams are reported in Ref. [46]). This represented an eight-fold increase in the effective surface area of the foam over the polished foil for the same electrode projection area. The initial foam surface showed more surface roughness compared to the polished surface of the foil (see Fig. S1a), which may be beneficial for enhanced surface adhesion of the formed NTs to the metal of the scaffolds. After anodisation, self-supported TiO_2 NTs were successfully grown on the outer and inner surfaces of the foam (see Fig. 1b and c).

Fig. 1f shows that the *I-t* transients recorded for the foam and the foil during anodisation under the same conditions (i.e., 35 V for 50 min with 0.45 M NH_4F) were distinctly different. Although a similar three-stage *I-t* profile (I, II and III as shown in Fig. 1f) was recorded for both the Ti foil and foam, the anodic *I* for the foam was substantially higher than for the foil, which could be attributed to the greater surface area provided by the foam leading to more surface reaction. Additionally, the *I-t* transients showed that both stage I and II (corresponding to the process of compact oxide formation and etching, respectively) completed sooner for the foam than the foil, which may suggest that a thinner compact oxide layer was initially formed on the foam surface and consequently the process to etch the layer (i.e., stage II) completed sooner.

Fig. 1d and e shows SEM images of as-grown TiO_2 NTs formed on the surface of the foil and the foam, respectively. Nanotubes grown on the foam and the foil had very different morphologies. Nanotubes grown on the outer surface of the foam had an average diameter and tube wall thickness of 45 ± 2.6 nm and 7.4 ± 1.0 nm in comparison to 60 ± 5.6 nm and 21 ± 5.9 nm for the foil. The smaller diameter and thinner tube wall of the NTs formed on the foam suggested that the effective anodisation voltage (i.e., the potential difference across the electrolyte/anode

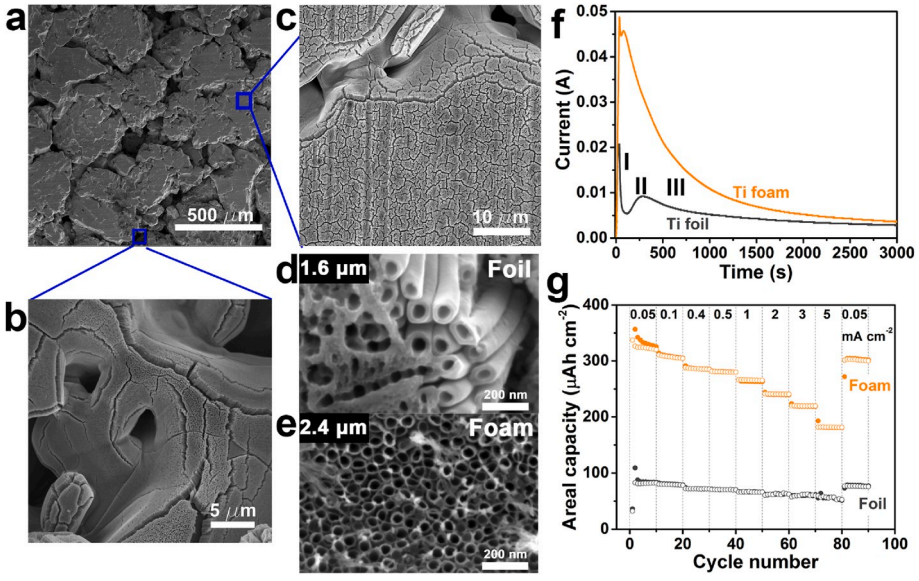

Fig. 1. (a) SEM image of a section of the foam after anodisation. (b, c) SEM images showing the formation of self-supported TiO_2 NTs on the (b) inner and (c) outer foam surfaces. (d, e) Top-view SEM images showing the different morphologies of NTs grown on a (d) foil and (e) foam after anodising with the same condition. (f) *I-t* transients for the foam and the foil recorded during anodisation using the same anodisation voltage of 35 V, respectively. (g) Areal capacities of TiO_2 NT electrodes prepared using a foam and a foil, values estimated from GCD measurements at current densities ranging from 0.05 to 5 mA cm^{-2}.

interface) was lower for the foam than the foil even though the overall applied anodisation voltages were the same for both cases. The lower voltage may result from larger *IR* losses across the electrolyte when anodising the foam caused by the higher anodic current as observed in Fig. 1f. The average tube length was 2.4 ± 0.07 μm for the foam (on outer surfaces), higher than 1.6 ± 0.09 μm for the foil; however shorter NTs with length < 1 μm were observed on inner foam surfaces (Fig. S1). This variability in tube length on the outer and inner foam surfaces is likely due to the limited access of electrolyte to the deeper pores of the foam during anodisation and the inhomogeneous electric field distribution on the different parts of the foam. Additionally, top-view SEM images show that, for the foil, the porous initiation oxide layer still present on top of organised NTs after 50 min of anodisation (Fig. 1d), whereas for the foam this layer has been completely removed and open tube tops were clearly exposed on the surface (Fig. 1e). The faster removal of the porous initiation oxide layer for the foam was consistent with the observation in Fig. 1f that the transition from stage II to III of the NT formation process occurred earlier for the foam than the foil.

The variability in morphology of NTs grown on the outer and inner foam surfaces makes it difficult to accurately estimate the volume and mass of TiO_2 NTs grown on Ti foams. Therefore, in this study, capacity values are reported in terms of per electrode projection area (i.e., Ah cm^{-2}) rather than per mass of the electroactive material (Ah g^{-1}). Mass estimates calculated using geometries of the NTs observed on the outer foam surface are provided in Table S3 in Supporting Information to allow for rough comparisons with other reports. The TiO_2 NT electrodes prepared using the foam and the foil were each coupled with a Li foil electrode and assembled into coin cells to assess their electrochemical performance. Fig. 1g compares the areal capacities of the foam and foil electrodes estimated from GCD measurements at a range of charging and discharging currents. The TiO_2 NT foam electrode demonstrated superior areal capacities, achieving ~320 μAh cm^{-2} at 0.05 mA cm^{-2} and ~181 μAh cm^{-2} at 5 mA cm^{-2}, in contrast to ~82 μAh cm^{-2} at 0.05 mA cm^{-2} and ~53 μAh cm^{-2} at 5 mA cm^{-2} obtained by the foil electrode. The improved areal capacities for the foam electrode at both low and high rates were most likely due to the higher per-electrode-area mass

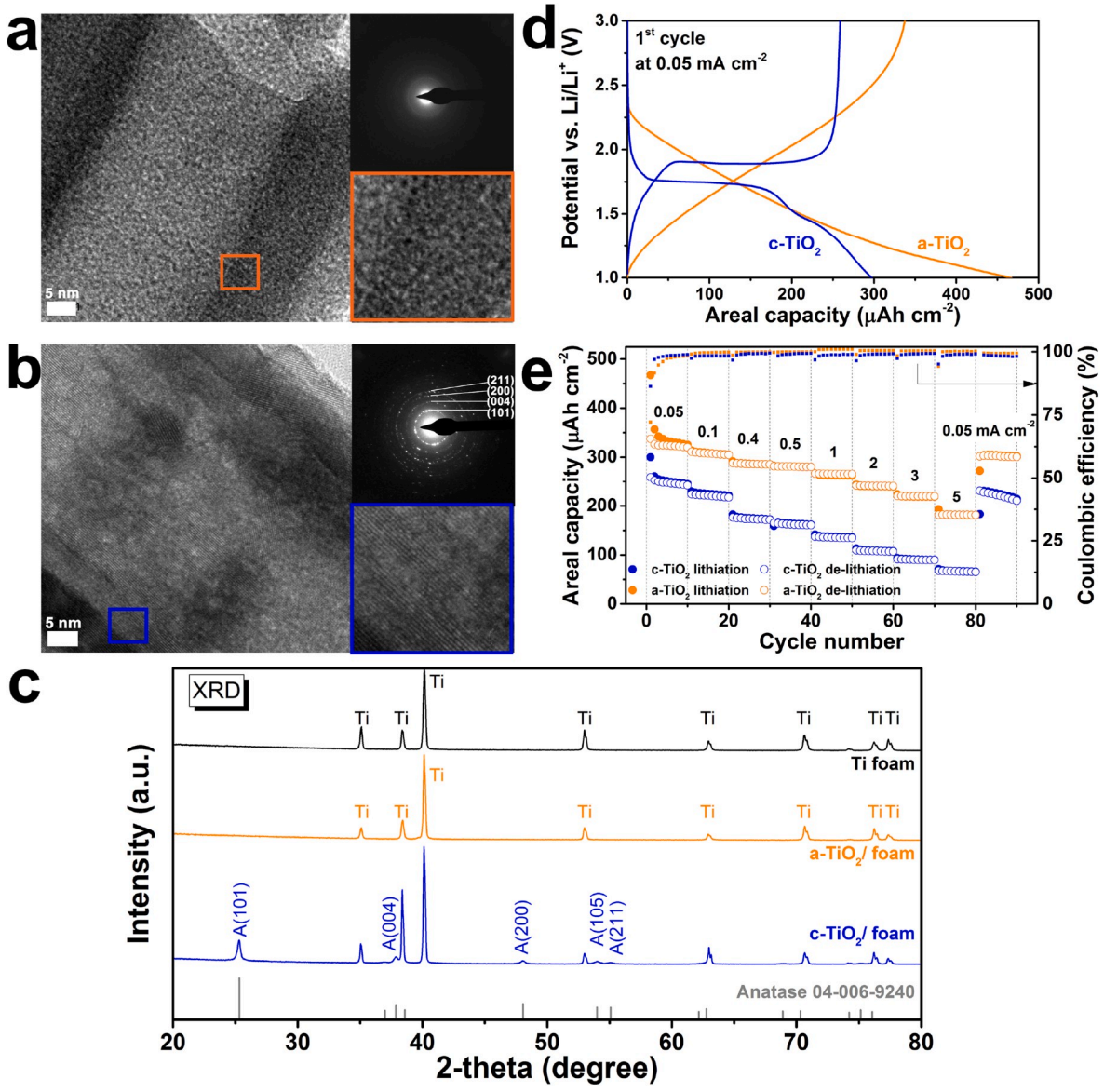

Fig. 2. (a, b) TEM images of (a) an as-anodised TiO_2 NT and (b) after annealing in air at 400 °C for 1 h, respectively. Magnified images of a local region and the SAED patterns are shown as insets in the TEM images. (c) XRD patterns of a Ti foam, as-anodised TiO_2 NTs and annealed TiO_2 NTs. (d) First-cycle lithiation and de-lithiation curves of the a-TiO_2 and c-TiO_2 NT electrodes. (e) Rate performance of the a-TiO_2 and c-TiO_2 NTs electrodes with capacity values being calculated from the GCD measurements at various current densities.

loading of TiO_2 on the foam than the foil scaffolds, which resulted from the larger effective surface area of the foam providing more reaction sites for NT growth during anodisation. However, the TiO_2 NT foam electrode showed a capacity retention of 57% at 5 mA cm^{-2} (normalised to the capacity at 0.05 mA cm^{-2}), slightly lower than 64% attained by the foil electrode. The lower capacity retention at high rates for the foam electrode may have been due to the restricted Li ion transport along the tortuous pathways presented in the foam, especially in the deeper pores/channels, and the influences from the different NT morphologies obtained by the foam and the foil electrodes. The influence of NT morphology on the areal capacity and rate capability of the foam electrodes are discussed further in Section 3.3.

3.2. Amorphous vs. crystalline NTs

Both a-TiO_2 and c-TiO_2 NTs electrodes were prepared from Ti foam scaffolds using the same anodisation conditions (i.e., 35 V, 50 min and 0.45 M NH_4F). Fig. 2a shows the TEM image of an as-grown NT. Lattice fringes are not evident in the TEM image (see Fig. 2a inset, bottom) and the SAED pattern is featureless (see Fig. 2a inset, top) indicating that the as-grown TiO_2 NTs were amorphous (at least long-range order was absent). After annealing at a temperature of 400 °C for 1 h, the initial NT morphology was retained (Fig. S2); however, the TiO_2 NTs were crystallised to the anatase phase ($I4_1/amd$) as evident by the lattice fringes in the TEM image and the diffraction rings in the SAED (see Fig. 2b). The crystallinity of the as-grown and annealed NTs was further confirmed by XRD shown in Fig. 2c as the anatase peaks only appeared in the diffraction patterns of the annealed TiO_2 NTs. Raman spectroscopy of the as-grown and annealed NTs are reported in Supporting Information Fig. S2.

The chemical composition of the a-TiO_2 and c-TiO_2 NTs electrodes was investigated using XPS. The Ti 2p core level spectra for both electrodes exhibits two peaks at binding energies of 464.4 eV and 458.8 eV, respectively (see Fig. S2d), confirming that the formed oxide before and after annealing were stoichiometric TiO_2 (at least for the surface). The O 1s core level spectra (Fig. S2e) reveal the presence of surface adsorbed O-containing species on both electrodes, including chemisorbed bridging hydroxyls (–OH) and physically adsorbed molecular water (H_2O) as evident by the peaks at ~531.6 and ~532.7 eV, respectively [52,53]. These surface hydroxyls and H_2O can react with the organic solvent and Li ions in the electrolyte leading to irreversible capacity losses during the initial cycles and/or capacity diminishing with battery cycling. Additionally, the F 1s core level spectra for the a-TiO_2 and c-TiO_2 NTs electrodes (Fig. S2f) exhibits a peak at ~684.5 eV, which corresponds to F^- physically adsorbed on TiO_2 surface or surface Ti–F species [54]. The a-TiO_2 NTs contained ~5.9 at% F estimated from the F1s spectrum, however this was reduced to less than ~1 at% after annealing at a temperature of 400 °C for 1 h. The reduced F concentration in TiO_2 NTs after annealing has been reported by several studies [55,56] and the decrease has been found to be proportional to the annealing temperature [56]. The presence of F in the TiO_2 NTs, in particular the F-rich layer at the bottom of the NTs, can weaken the adhesion of NTs to the Ti metal substrate and therefore may affect the cycle life of the electrode [57,58]. The XPS results revealed that the concentration of both O- and F-containing surface species were higher in a-TiO_2 than c-TiO_2 NTs. The effects of these surface contaminants on the Coulombic efficiency and cyclability of the a-TiO_2 and c-TiO_2 NTs electrodes are discussed in the next section.

The prepared a-TiO_2 and c-TiO_2 NTs foam electrodes were coupled with Li foil electrodes and assembled into coin cells for electrochemical characterisation. Fig. 2d shows the first lithiation and de-lithiation curves of the a-TiO_2 and c-TiO_2 NTs electrodes, measured at a current density of 0.05 mA cm^{-2}. The c-TiO_2 NTs electrode (blue curves) showed two well-defined plateaus at potentials of ~1.75 and ~1.9 V in its lithiation and delithiation, respectively, which correspond to phase transitions between Li-poor Li_xTiO_2 ($0.01 < x \leq 0.21$) with the tetragonal anatase structure ($I4_1/amd$) to the orthorhombic Li-titanate ($Li_{\sim 0.55}TiO_2$) phase (*Imma*) [59]. These plateau potentials are in good agreement with previously reported values for c-TiO_2 electrodes [39,47,60,61]. In addition to the dominant plateaus, an additional lithiation plateau was evident at ~1.46 V for c-TiO_2. This potential plateau has been observed for TiO_2 crystallites with a size <7 nm and has been attributed to a second phase transition to a fully-lithiated $LiTiO_2$ ($I4_1/amd$) at this potential [59,62].

In contrast, these voltage plateaus were absent in the lithiation/delithiation curves for the a-TiO_2 electrode (orange curves) and instead, the voltage of the electrode changed almost linearly with the capacity suggesting a capacitor-like Li ion storage mechanism [63–65]. Xiong et al. reported a characteristic plateau at ~0.9 V vs. Li/Li^+ in the first lithiation curve for the a-TiO_2 NT electrode and the authors attributed this plateau to an irreversible structural transformation from amorphous TiO_2 to a face-centred-cubic crystalline structure upon uptake of Li ions [45]. However, this voltage plateau was not observed in our first lithiation curve for the a-TiO_2 NT electrode (and also a number of other studies [21,40,45]), possibly due to a cycling potential range of 1–3 V vs. Li/Li^+ being used in this study. A lithiation potential of <1 V may be required for the structural change observed by Xiong et al. [45].

Cyclic voltammetry measurements were performed for the a-TiO_2 and c-TiO_2 NT electrodes with scan rates ranging from 0.05 to 100 mV s^{-1} and the results were reported in Supporting Information Fig. S3. For the c-TiO_2 electrode, its CV curves evidently show two pairs of sharp peaks (main peaks at 1.73 and 2.0 V and small peaks at 1.46 and 1.7 V) indicating the potentials at which phase transitions occurred in c-TiO_2 during Li ion insertion and extraction. These peak potentials agree well with the plateau positions evident in the GCD curves of the c-TiO_2 electrode. However, such narrow peaks were absent in the CV curves of the a-TiO_2 electrode and instead, two broad humps over a wide range of potential were observed. The absence of sharp CV peaks in a-TiO_2 may have been due to the non-uniform distribution of free spaces in the highly disordered and defective structures of the amorphous material leading to a broad potential range for Li ion insertion and extraction [39,66]. To understand the charge storage mechanism for these two oxides, scan-rate dependent CV analysis to extract the *b*-values was performed [20,48,49,67]. Fig. S3c in Supporting Information plots the logarithm of the anodic peak current, I_p, as a function of the logarithm of the voltage scan rate, v, from which the *b*-values were estimated from the slopes of the fitted lines to these plots according to Eq. (2.1). A *b*-value of 0.50 was obtained for the c-TiO_2 suggesting its Li ion insertion/extraction process was diffusion controlled. In contrast, a *b*-value of 0.96 was estimated for the a-TiO_2 implying that Li ion storage in the amorphous matrix was predominantly a capacitive process. It worth clarifying that the term 'capacitive' in this study refers to any non-diffusion limited processes, which include electrochemical double layer storage [68,69], surface pseudocapacitive storage [70] and bulk-insertion pseudocapacitive storage [71,72]. Considering the NT morphology and therefore the electrode surface area were similar between the a-TiO_2 and c-TiO_2 electrodes, differences in the charge storage mechanism identified by the *b*-value analysis are unlikely to be explained solely by surface storage processes. In fact, recent studies have identified insertion pseudocapactive storage behaviour for Li ion storage in a-TiO_2 [64,73] and this has been attributed to the fast Li ion diffusion properties in the amorphous oxide matrix [73].

Fig. 2e compares the rate performance of the a-TiO_2 and c-TiO_2 NTs electrodes with capacity values being calculated from the GCD measurements at current densities ranging from 0.5 to 5 mA cm^{-2}. The a-TiO_2 electrode demonstrated superior rate performance to the c-TiO_2 electrode, with capacities of ~320 μAh cm^{-2} at 0.05 mA cm^{-2} and ~181 μAh cm^{-2} at 5 mA cm^{-2} being attained, in contrast to ~242 μAh cm^{-2} at 0.05 mA cm^{-2} and ~65 μAh cm^{-2} at 5 mA cm^{-2} for the c-TiO_2 electrode. The improved rate performance in a-TiO_2 electrodes has been attributed to: (i) highly reversible surface film reactions [47]; and (ii) enhanced Li ion diffusion and interfacial charge transfer rates in amorphous over

anatase forms [73]. Jiang et al. showed that the chemical diffusion coefficient of Li ions in a-TiO_2 can be two orders of magnitude larger than those in c-TiO_2 [73]. The faster Li ion diffusion in a-TiO_2 may benefit from the absence of long-range ordering and the loosely packed and disordered structure of a-TiO_2, which provide more free space and open spatial channels than available in c-TiO_2 (anatase). This can enable facile diffusion pathways for Li ion transport [64]. This study also revealed that not only is Li ion diffusion faster in the a-TiO_2, but the interfacial charge transfer may also occur more rapidly in the amorphous material further contributing to its superior rate performance. The improved interfacial charge transfer kinetics at amorphous surfaces has also been observed for $LiFePO_4$ by Kang and Ceder, who reported enhanced charging/discharging rates for $LiFePO_4$ electrodes by coating crystalline $LiFePO_4$ particles with an amorphous film [74]. The surface of anatase TiO_2 is also anisotropic and Li ion insertion and diffusion is more facile along the [001] direction [61]. One possibility is that the amorphous surface of a-TiO_2 NTs minimises the anisotropy of the surface properties and facilitates delivery of Li ions into the matrix of the metal oxide, whilst for c-TiO_2 ions need to diffuse laterally across the crystalline surface before their position coincides with a crystal channel into which they can 'enter'.

The a-TiO_2 electrode had an irreversible capacity loss of 28% during the first charge/discharge cycle in comparison to 14% for the c-TiO_2 electrode. This higher irreversible capacity loss may have been due to the higher concentration of OH and H_2O species on the surfaces of the a-TiO_2 NT (as evident from the XPS measurements and reported above), which contributed to more irreversible surface reactions with the electrolyte during the initial cycles. However, the Coulombic efficiency increased from 72% to 86% for the a-TiO_2 and c-TiO_2 electrode, respectively, to ~99% after the first 10 cycles suggesting that these irreversible side reactions at the NT surface only occurred during the initial cycles and did not affect the long-term cyclability of these electrodes. The long-term cyclability of the a-TiO_2 NT electrodes is further investigated in Section 3.4.

3.3. Influence of anodisation parameters and NT geometry

The morphology of TiO_2 NTs grown on Ti foams and the capacity and rate capability of formed electrodes were sensitive to the anodisation conditions, in particular: i) anodisation voltage; ii) anodisation duration; and iii) NH_4F concentration. Fig. 3a–c graphs the geometries of NTs formed on Ti foam surfaces as a function of each of the above three anodisation parameters. In all cases, the geometric parameters of the NTs were measured from SEM images of the NT foam electrodes (see Supporting Information Fig. S4-6). Fig. 3a shows that anodisation voltage had a significant effect on the inner diameter and length of NTs however a small impact on the wall thickness. The inner diameter and tube length of the NTs increased significantly from 23 nm to 42 nm and 0.6 μm–3.2 μm, respectively, as the anodisation voltage increased from 12.5 V to 40 V. This observation is consistent with previous reports on NTs formed on foils [75–78]. The NT growth process is essentially a competition between electrochemical oxidation and dissolution [79]. At higher anodisation voltages, the electric field driving force, which facilitates ion migration through the oxide, is enhanced and this may have led to faster electrochemical reactions leading to the pores growing faster both laterally (larger NT diameter) and vertically (longer tubes).

Fig. 3b shows that the anodisation duration affected most significantly the length of NTs but had a negligible impact on the wall thickness. The NTs grew rapidly in length during the initial stage of anodisation, however growth then slowed and after 100 min of anodisation and no further increases in NT length were evident. This limiting tube length (3.4 μm after anodising the foam with a voltage of 35 V for 5 h) indicated the onset of an equilibrium between the NT growth and chemical dissolution of the formed oxide. A slight increase in NT inner diameter with the anodisation duration was evident, which may be due to the accumulation of reaction products during anodisation leading to

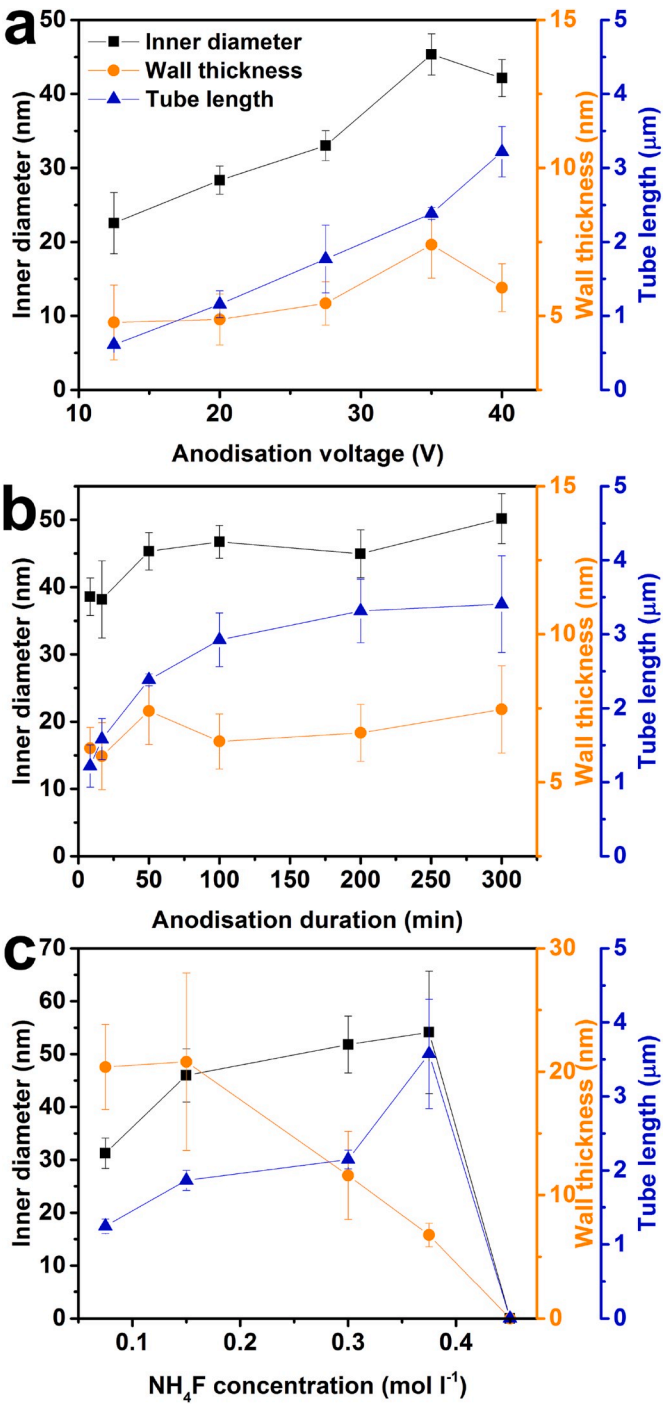

Fig. 3. Geometric properties of as-grown TiO_2 NTs formed on Ti foams as a function of (a) anodisation voltage, (b) anodisation duration and (c) NH_4F concentration.

increased electrolyte conductivity and consequently a higher effective voltage across the foam and electrolyte interface [80,81]. For anodisation durations exceeding 100 min, grass-like surface structures were observed (see Fig. S5) which resulted from the collapsing and aggregation of NT tops as the tube walls became too thin to support their weight or withstand the capillary forces during drying. The formation of aggregated NT tips seemed to occur earlier for foam compared to foil substrates (typically observed when tube length is more than several tens of micrometres for foils [82]). The earlier aggregation of NT tips may occur due to the curvature of the foam surface.

Fig. 3c shows that increasing the NH_4F concentration in the

electrolyte from 0.075 M to 0.375 M led to an increase in the NT inner diameter (31–54 nm) and length (1.2–3.6 μm) however a reduction in the wall thickness (20 nm–6.8 nm). The presence of F ions in the electrolyte is essential for the formation of NTs and its concentration can significantly affect the rate of chemical dissolution of the formed TiO_2 [79,81,83]. Increases in the NH_4F concentration effectively accelerated etching of the formed NT walls thereby leading to decreases in the wall thickness but increases in the inner diameter of NTs. The increase in tube length with a higher NH_4F concentration is likely due to the higher F content enabling: i) a thinner barrier oxide and therefore a stronger electrochemical driving force that facilitates ion migration through the oxide for faster pore growth; ii) additional lengthening of NTs by the plastic flow mechanism due to the enhanced electric field and ion movement [84,85]; and iii) improved electrolyte conductivity leading to a higher potential difference across the anode and electrolyte interface [86]. Additionally, the F ion concentration also affected the surface morphology of the formed NTs. For NH_4F concentrations at 0.075 M and 0.15 M, a porous oxide remained on the surface due to the slower oxide dissolution by F ions (see Fig. S6). This porous surface layer was partially and completely removed at an NH_4F concentration of 0.3 M and 0.375 M, respectively. However, further increasing the NH_4F concentration to 0.45 M led to excessively fast etching of the formed NTs and no NTs were observed on the foam surface.

To determine the effect of NT geometry on the areal capacity and rate capability of the electrodes, a-TiO_2 NT foam electrodes prepared using different anodisation parameters were assembled into coin cells for GCD tests. Fig. 4(a-c) show areal capacities of each of the a-TiO_2 NT foam electrodes as a function of the current density and capacities were estimated from GCD measurements at current densities from 0.05 to 5 mA cm^{-2}. Fig. 4d-f graph the normalised capacity (normalised to the corresponding capacity measured at the lowest rate) of each of the TiO_2 NT foam electrodes as a function of the charge/discharge rate, *R*, which

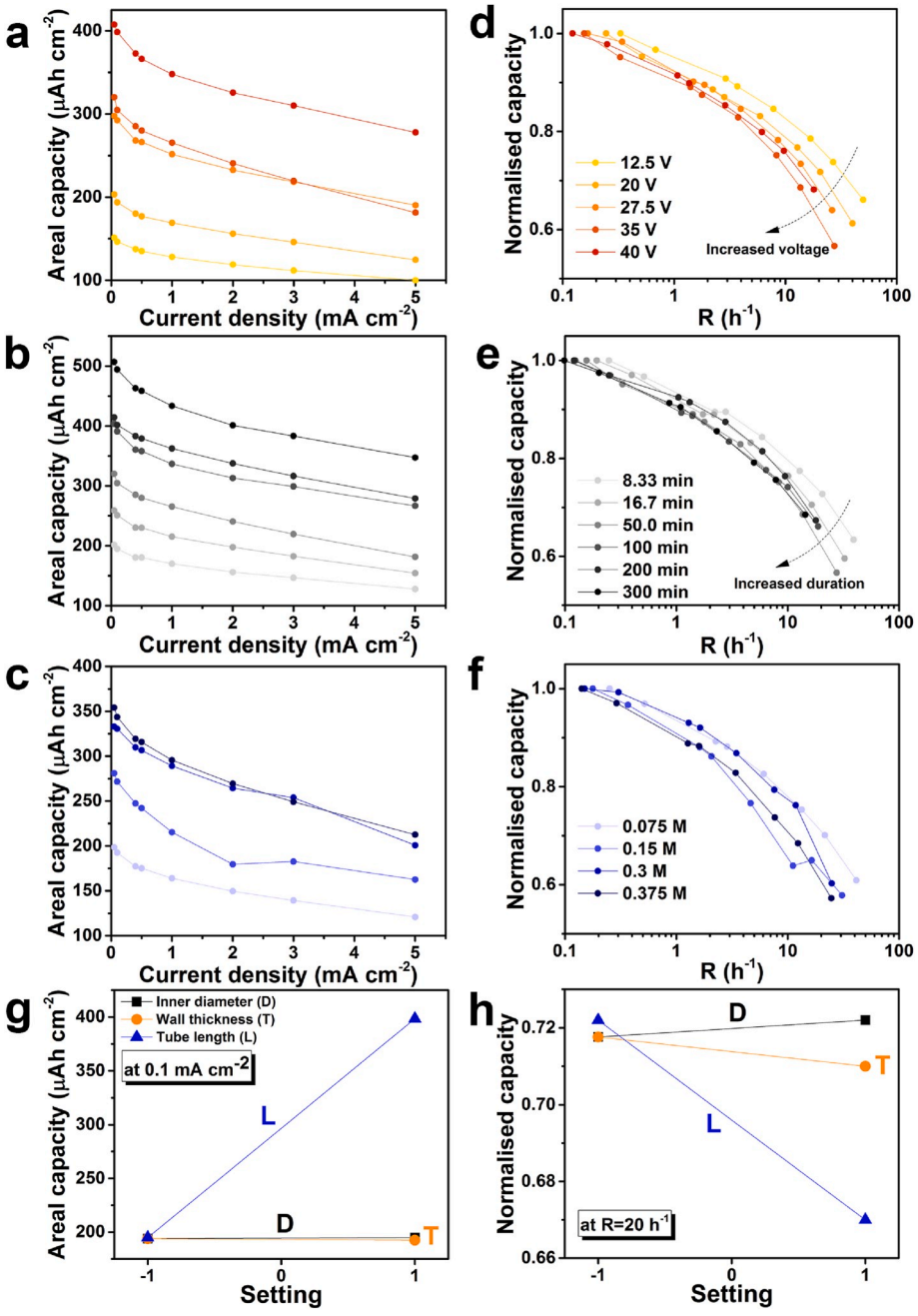

Fig. 4. (a–c) Areal capacity of TiO_2 NT foam electrodes prepared with different (a) anodisation voltage, (b) anodisation duration and (c) NH_4F concentration. (d–f) Normalised capacity as a function of the rate parameter *R* for TiO_2 NT electrodes prepared with differnet (d) anodisation voltage, (e) anodisation duration and (f) NH_4F concentration; the capacities were normalised to the areal capacity of the same electrode measured at the lowest current density of 0.05 mA cm^{-2}. (g, h) Main effect tests for (g) the electrode areal capacities measured at 0.1 mA cm^{-2} and (h) the normalised capacity measured at $R = 20$ h^{-1}.

is introduced and defined in Section 2.3. Higher electrode areal capacities were achieved by increasing the anodisation voltage (see Fig. 4a) and increasing anodisation duration (see Fig. 4b). Conversely, increasing the anodisation voltage deteriorated the rate performance of the NT foam electrodes (see Fig. 4d). A similar trend is observed for the anodisation duration (i.e., the electrode rate capability degraded as the anodisation duration increased from 8.3 to 100 min), however increases in the anodisation duration beyond 100 min only slightly affected the rate performance (see Fig. 4e). The electrode where anodisation was performed for 200 min seemed to deviate from this trend possibly due to variations in the foam geometries which also affect the rate performance of the NT electrodes. Fig. 4c shows that the electrode areal capacity increased gradually as the NH_4F concentration was increased from 0.075 M to 0.375 M. However, the rate performance of the NT electrodes appears to degrade as the NH_4F concentration was increased from 0.075 M to 0.375 M (Fig. 4f).

Understanding the dependence of the electrode areal capacity and rate capability on the geometric properties of NTs is not straightforward as varying anodisation conditions lead to changes in more than one geometric parameter of the formed NTs. To determine which of the three geometric parameters of NTs has the dominant effect on capacity and rate performance (i.e., inner diameter, wall thickness and tube length), a statistical 'main effect' test was performed. The 'main effect' test plots the response (i.e., areal capacity and rate capability) as a function of a single factor at two significantly divergent settings (the '-1' and '+1' settings indicate the lower and upper bound values, respectively) whilst keeping the other factors relatively unchanged. Fig. 4g shows the 'main effect' plot for the areal capacity of TiO_2 NT foam electrodes measured at a current density of 0.1 mA cm^{-2}. The electrode areal capacity was dominantly affected by the tube length but had negligible dependence on the inner diameter or wall thickness of the NTs, suggesting that the tube length was the 'primary' factor in affecting the areal capacity of the TiO_2 NT foam electrodes. This suggests that the trends noted from Fig. 4a–c that electrode areal capacity increased with an increasing NH_4F concentration, anodisation voltage or duration were most likely due to the longer tube length attained at higher values of these parameters.

Fig. 4h shows the 'main effect' plot for the normalised capacity of TiO_2 NT foam electrodes measured at a rate of $R = 20\ h^{-1}$. Tube length was evidently the 'primary' factor and had a negative effect on the rate performance of the electrodes. The wall thickness seemed to have a smaller and negative effect on the rate performance whereas the inner diameter had almost negligible influence. The main effect rate analysis suggested that, since the NT wall thickness was almost constant for the different anodisation voltages, the degraded rate capability of electrodes fabricated with increasing anodisation voltage in Fig. 4d was most likely due to the increase in tube length from 0.6 μm at 12.5 V to 3.2 μm at 40 V. The increase in tube length can lead to a higher electrical resistance in the NTs and possibly a higher TiO_2/Ti contact resistance due to the poorer interfacial adhesion of NTs to the Ti substrate as commonly observed for longer NTs [29]. Both of these factors would have increased electrode impedance at high rates. Similarly, the poorer rate capability of the electrodes with a longer anodisation duration as evident in Fig. 4e may have arisen from the two-fold increase in tube length as the anodisation duration increased from 8.3 to 100 min. Further extending the anodisation duration from 100 min to 300 min only slightly increased the tube length (see Fig. 3b) thereby resulting in similar rate performance in the electrodes. For the investigation on the NH_4F concentration, the observed degradation in the electrode rate performance as the NH_4F increased from 0.075 M to 0.15 M may also be attributed to the increase in tube length at a higher NH_4F concentration. Interestingly, an enhanced rate performance was evident when further increasing the NH_4F concentration to 0.3 M. This improvement may have benefited from reductions in the NT wall thickness at higher NH_4F concentrations (see Fig. 3c). Thinner NT walls have been reported to reduce the distance for Li ion diffusion in TiO_2 NTs and therefore may be beneficial for electrode rate performance [44]. This conclusion is consistent with the 'main effect' test in Fig. 4h. The changes in electrode rate capability with NH_4F concentration may have been influenced by the trade-off between the tube length and wall thickness which had opposite correlations with the NH_4F concentration. Additionally, the unexpected improvement in the electrode rate performance at an NH_4F concentration of 0.3 M compared to 0.15 M may also be partly due to the complete removal of the porous surface layer (see Supporting Information Fig. S6), which can impede Li ion access to the underneath NTs.

The analysis in this section suggests that the areal capacity and rate capability of a-TiO_2 NT foam electrodes are predominantly affected by the tube length, with the wall thickness possibly having a weaker and negative influence on the rate performance of the electrodes. Although longer NTs are beneficial to improve the electrode areal capacity, they typically lead to poorer rate performance presumably due to the greater *IR* losses in the electrode introduced by the additional resistance in the longer NTs and the increased contact resistance of NTs to the Ti scaffolds.

3.4. Comparisons to previous studies

Fig. 5a shows the areal capacity as a function of the charge current density for the a-TiO_2 NT foam electrodes prepared in this study in comparison to previously reported values obtained for anodised TiO_2 NT electrodes fabricated using foils or foams. Evidently, the areal capacity and rate performance of TiO_2 NT electrodes depend significantly on: i) the NT tube length; ii) the crystallographic structure of TiO_2 (amorphous or crystalline); and iii) the geometry of metal scaffolds (foam or foil). Although there are discrepancies in the reported capacities by different studies possibly due to variations in their anodisation or coin cell assembly processes, in general, longer tubes yield greater areal capacity by increasing the mass loading of the electroactive TiO_2 per electrode area, however, they also lead to reduced capacity retention at high rates. TiO_2 NT electrodes fabricated using porous Ti foams (open symbols in Fig. 5a), including the electrodes reported in this study, generally exhibit greater capacity retention at high rates than electrodes prepared using planar foils (closed symbols). The large surface area of the foam scaffolds enables a high per-area mass loading of the electroactive TiO_2 for high areal capacities whilst retaining a short NT length for improved rate performance. By adopting the strategies of using porous Ti foams, a-TiO_2, and optimised anodisation conditions as determined from Section 3.3 (0.45 M NH_4F, 35 V and 300 min), the a-TiO_2 NT foam electrodes fabricated in this study achieved not only a high areal capacity of 507 μAh cm^{-2} at 50 μA cm^{-2} with a tube length of only ~3.4 μm but also excellent capacity retention at high rates (347 μAh cm^{-2} at 5 mA cm^{-2}). Such rate performance represents a significant improvement over previously reported values for TiO_2 NTs electrodes fabricated using foils or foams with tube length <32 μm. Our enhanced rate performance benefited from the use of high surface area foam current collectors, the amorphous host structure which enables faster Li ion storage kinetics [73] and short NTs which allow for increased electronic conductivity. Although substantially higher areal capacities above 2 mAh cm^{-2} can be achieved by the growth of ultra-long NTs on a foil with a tube length >45 μm [28,29], these electrodes suffered from poor capacity retention at high rates and, more importantly, significant capacity degradation over cycling as shown in Fig. 5b (capacity retention < 45% within the first 50th cycles).

Additionally, the cycling stability of the NT electrodes was also compromised with very long tube lengths possibly due to a poorer surface adhesion between the long NTs and the Ti current collectors [29]. Fig. 5b shows that the a-TiO_2 NT foam electrodes prepared in this study demonstrated excellent cycling stability, attaining 83% of its peak capacity after 2000 cycles when measured at a current density of 0.5 mA cm^{-2}. The use of a-TiO_2 rather than c-TiO_2, despite the higher concentration of surface contaminants in the amorphous oxide (as evident in the XPS results in Section 3.2), did not seem to affect the long-term

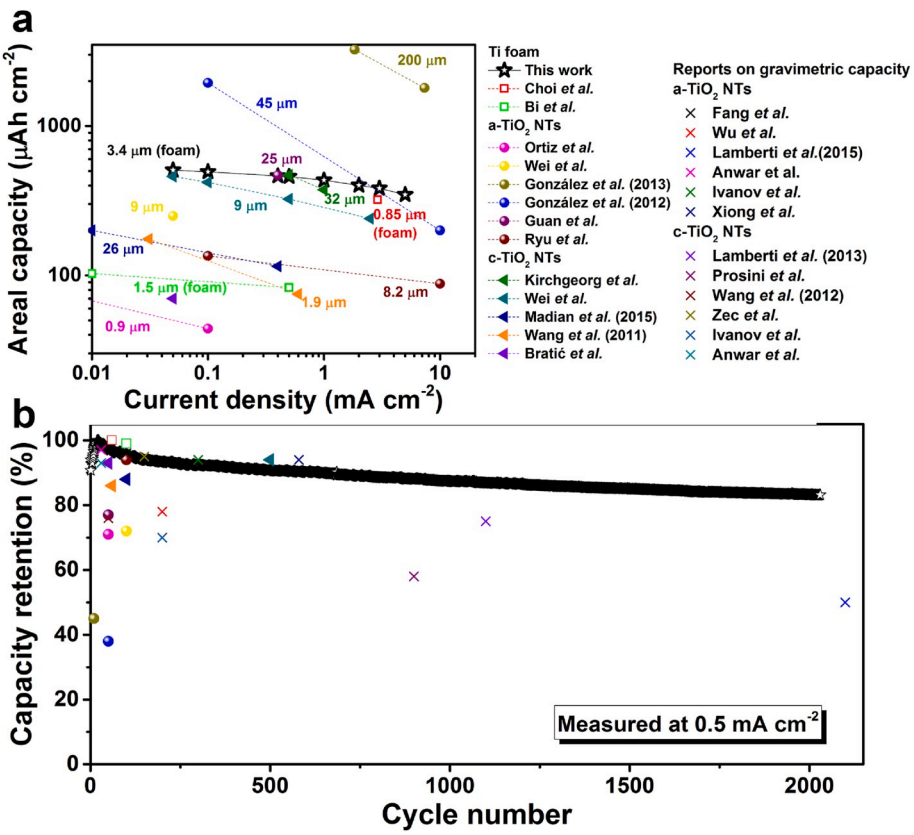

Fig. 5. Comparison of the (a) rate performance and (b) cycling stability between the a-TiO_2 NT foam electrode prepared in this study and previously reported anodised TiO_2 NT electrodes. Literature data were obtained from NT electrodes prepared using Ti foams (Choi et al. [43] and Bi et al. [42], open symbols), or foils (Ortiz et al. [26], Wei et al. [27], González et al. (2013) [29], González et al. (2012) [28], Guan et al. [30], Ryu et al. [31], Kirchgeorg et al. [32], Madian et al. [87], Wang et al. (2011) [33] and Bratić et al. [34], closed symbols). Additional data in (b) were obtained from studies reporting gravimetric capacity (Fang et al. [39], Wu et al. [66], Lamberti et al. (2015) [40], Anwar et al. [88], Ivanov et al. [89], Xiong et al. [45], Lamberti et al. (2013) [90], Prosini et al. [91], Wang et al. (2012) [92] and Zec et al. [93]). The inserted labels in (a) indicate the NT length reported in each study. In (b), the electrode capacities were normalised to the peak capacity in the initial cycles. See Table S1 and S2 for detailed information.

cyclability of the electrode. The superior cycling stability achieved by the electrode prepared in this study compared to previously reported TiO_2 NT electrodes may be attributed to the initial rough surface of the foam scaffold and the short tube length of the NTs, both of which facilitated a stronger surface adhesion of the NTs to the metal of the current collector thereby enabling the excellent structural stability of the electrode upon prolonged cycling.

4. Conclusions

In this study, we demonstrated that excellent areal capacity, rate capability and long-term cyclability can be achieved using TiO_2 NT electrodes using a concurrent optimisation strategy involving the: i) geometry of the metal scaffolds, ii) crystallographic structure of TiO_2; and iii) geometry of formed NTs. The use of porous Ti foams as current collecting scaffolds to support TiO_2 NTs for Li ion storage has demonstrated several key advantages over Ti foils. These advantages include: i) a porous metal network facilitating electrolyte access to a larger surface area for faster NT growth; ii) a large surface area enabling a high loading mass of TiO_2 without unfavourable increases in tube length; and iii) an initial rough surface facilitating stronger adhesion of the NTs to the metal surface for a lower contact resistance and improved cycling stability. Furthermore, it was shown that a-TiO_2 NT electrodes exhibit superior rate performance compared to their c-TiO_2 counterparts. This can be attributed to the distinct charge storage mechanism and faster kinetics resulting from the loose atomic packing and disordered surface of the amorphous oxide. Although more 'contaminants' (e.g., OH, H_2O and F) remain on the surface of the a-TiO_2 electrodes after anodisation and reduce their initial Coulombic efficiencies, these surface species do not degrade the long-term cyclability of these electrodes.

It was shown that the NT wall thickness is mostly determined by the NH_4F concentration whereas anodisation voltage, duration and NH_4F concentration all affect the inner diameter and length of the NTs. Main effect analyses suggested that the areal capacity and rate capability of the a-TiO_2 NT electrodes is predominately dependent on the tube length with inner diameter having little effect. The rate performance of the a-TiO_2 NT electrodes is also negatively affected by the wall thickness of the NTs, however this effect is relatively small compared to that of tube length. Although longer tube lengths are preferable for higher areal capacity, they typically lead to poorer rate capability and cyclability of the electrode. This presents a compromise for the achievement of both high capacity and high capacity retention at high cycling rates.

By adopting the strategies of using high surface area Ti foams, an amorphous host structure and optimised NT geometries, we show that a-TiO_2 NT foam electrodes can achieve a high areal capacity of 507 μAh cm^{-2} at 50 μA cm^{-2} but also excellent rate capability (retained a capacity of 347 μAh cm^{-2} at 5 mA cm^{-2}) and long-term cycling stability with capacity retention of 83% after 2000 cycles. This study demonstrates the potential advantages of using a-TiO_2 foam electrodes as the anodes for high-rate LIBs through promising preliminary results using coin cells. Practical LIB applications would also require the consideration of the electrode size, mass loading of the electroactive material and usage of Li in batteries. Further investigation is needed to explore some of these aspects and understand the practical potential of these a-TiO_2 foam anodes.

Declaration of competing interest

The authors declare that they have no known competing financial interests or personal relationships that could have appeared to influence the work reported in this paper.

CRediT authorship contribution statement

Yu Jiang: Conceptualization, Methodology, Formal analysis, Investigation, Writing - original draft. **Charles Hall:** Investigation. **Patrick A. Burr:** Methodology, Writing - review & editing. **Ning Song:** Investigation. **Derwin Lau:** Investigation. **Jodie Yuwono:** Software, Validation.

Da-Wei Wang: Resources, Writing - review & editing. **Zi Ouyang:** Supervision, Writing - review & editing. **Alison Lennon:** Supervision, Writing - review & editing, Funding acquisition.

Acknowledgements

This work has been supported by the Australian Research Council through Discovery Grant DP170103219 "Advanced Electrochemical Capacitors". The first author would like to acknowledge the support of the Australian government through their Research Training Program scholarships.

Appendix A. Supplementary data

Supplementary data related to this article can be found at https://doi.org/10.1016/j.jpowsour.2020.228205.

References

[1] A. Lennon, Y. Jiang, C. Hall, D. Lau, N. Song, P. Burr, C.P. Grey, K.J. Griffith, High-rate lithium ion energy storage to facilitate increased penetration of photovoltaic systems in electricity grids, MRS Energy Sustain. 6 (2019) E2.
[2] Y. Jiang, J. Fletcher, P. Burr, C. Hall, B. Zheng, D.-W. Wang, Z. Ouyang, A. Lennon, Suitability of representative electrochemical energy storage technologies for ramp-rate control of photovoltaic power, J. Power Sources 384 (2018) 396–407.
[3] Z.P. Cano, D. Banham, S. Ye, A. Hintennach, J. Lu, M. Fowler, Z. Chen, Batteries and fuel cells for emerging electric vehicle markets, Nat. Energy 3 (2018) 279–289.
[4] S.J. An, J. Li, C. Daniel, D. Mohanty, S. Nagpure, D.L. Wood, The state of understanding of the lithium-ion-battery graphite solid electrolyte interphase (SEI) and its relationship to formation cycling, Carbon 105 (2016) 52–76.
[5] E. Peled, S. Menkin, Review—SEI: past, present and future, J. Electrochem. Soc. 164 (2017) A1703–A1719.
[6] A. Wang, S. Kadam, H. Li, S. Shi, Y. Qi, Review on modeling of the anode solid electrolyte interphase (SEI) for lithium-ion batteries, npj Comput. Mater. 4 (2018) 15.
[7] L. Somerville, J. Bareño, S. Trask, P. Jennings, A. McGordon, C. Lyness, I. Bloom, The effect of charging rate on the graphite electrode of commercial lithium-ion cells: a post-mortem study, J. Power Sources 335 (2016) 189–196.
[8] G. Ning, B. Haran, B.N. Popov, Capacity fade study of lithium-ion batteries cycled at high discharge rates, J. Power Sources 117 (2003) 160–169.
[9] M. Broussely, P. Biensan, F. Bonhomme, P. Blanchard, S. Herreyre, K. Nechev, R. J. Staniewicz, Main aging mechanisms in Li ion batteries, J. Power Sources 146 (2005) 90–96.
[10] Q. Liu, C. Du, B. Shen, P. Zuo, X. Cheng, Y. Ma, G. Yin, Y. Gao, Understanding undesirable anode lithium plating issues in lithium-ion batteries, RSC Adv. 6 (2016) 88683–88700.
[11] K. Liu, Y. Liu, D. Lin, A. Pei, Y. Cui, Materials for lithium-ion battery safety, Sci. Adv. 4 (2018), eaas9820.
[12] M. Wagemaker, G.J. Kearley, A.A. van Well, H. Mutka, F.M. Mulder, Multiple Li positions inside oxygen octahedra in lithiated TiO_2 anatase, JACS 125 (2003) 840–848.
[13] N. Nitta, F. Wu, J.T. Lee, G. Yushin, Li-ion battery materials: present and future, Mater. Today 18 (2015) 252–264.
[14] X. Su, Q. Wu, X. Zhan, J. Wu, S. Wei, Z. Guo, Advanced titania nanostructures and composites for lithium ion battery, J. Mater. Sci. 47 (2012) 2519–2534.
[15] M. Madian, A. Eychmüller, L. Giebeler, Current advances in TiO_2-based nanostructure electrodes for high performance lithium ion batteries, Batteries 4 (2018) 7.
[16] D.G.E. Peled, J. Penciner, The anode/electrolyte interface, in: C. Daniel, J. O. Besenhard (Eds.), Handbook of Battery Materials, Wiley-VCH Verlag GmbH & Co. KGaA, 2011.
[17] M.D. Earle, The electrical conductivity of titanium dioxide, Phys. Rev. 61 (1942) 56–62.
[18] O. Rhee, G. Lee, J. Choi, Highly ordered TiO_2 microcones with high rate performance for enhanced lithium-ion storage, ACS Appl. Mater. Interfaces 8 (2016) 14558–14563.
[19] C. Jiang, M. Wei, Z. Qi, T. Kudo, I. Honma, H. Zhou, Particle size dependence of the lithium storage capability and high rate performance of nanocrystalline anatase TiO2 electrode, J. Power Sources 166 (2007) 239–243.
[20] J. Wang, J. Polleux, J. Lim, B. Dunn, Pseudocapacitive contributions to electrochemical energy storage in TiO_2 (anatase) nanoparticles, J. Phys. Chem. C 111 (2007) 14925–14931.
[21] W.J.H. Borghols, D. Lützenkirchen-Hecht, U. Haake, W. Chan, U. Lafont, E. M. Kelder, E.R.H. van Eck, A.P.M. Kentgens, F.M. Mulder, M. Wagemaker, Lithium storage in amorphous TiO_2 nanoparticles, J. Electrochem. Soc. 157 (2010) A582–A588.
[22] J. Zheng, G. Ji, P. Zhang, X. Cao, B. Wang, L. Yu, Z. Xu, Facile aluminum reduction synthesis of blue TiO2 with oxygen deficiency for lithium-ion batteries, Chem. Eur J. 21 (2015) 18309–18315.
[23] J. Zheng, L. Liu, G. Ji, Q. Yang, L. Zheng, J. Zhang, Hydrogenated anatase TiO2 as lithium-ion battery anode: size–reactivity correlation, ACS Appl. Mater. Interfaces 8 (2016) 20074–20081.
[24] J. Zheng, Y. Liu, G. Ji, P. Zhang, X. Cao, B. Wang, C. Zhang, X. Zhou, Y. Zhu, D. Shi, Hydrogenated oxygen-deficient blue anatase as anode for high-performance lithium batteries, ACS Appl. Mater. Interfaces 7 (2015) 23431–23438.
[25] K. Lee, A. Mazare, P. Schmuki, One-dimensional titanium dioxide nanomaterials: nanotubes, Chem. Rev. 114 (2014) 9385–9454.
[26] G.F. Ortiz, I. Hanzu, T. Djenizian, P. Lavela, J.L. Tirado, P. Knauth, Alternative Li-ion battery electrode based on self-organized titania nanotubes, Chem. Mater. 21 (2009) 63–67.
[27] W. Wei, G. Oltean, C.-W. Tai, K. Edström, F. Björefors, L. Nyholm, High energy and power density TiO_2 nanotube electrodes for 3D Li-ion microbatteries, J. Mater. Chem. 1 (2013) 8160–8169.
[28] J.R. González, R. Alcántara, F. Nacimiento, G.F. Ortiz, J.L. Tirado, E. Zhecheva, R. Stoyanova, Long-length titania nanotubes obtained by high-voltage anodization and high-intensity ultrasonication for superior capacity electrode, J. Phys. Chem. C 116 (2012) 20182–20190.
[29] J.R. González, R. Alcántara, G.F. Ortiz, F. Nacimiento, J.L. Tirado, Controlled growth and application in lithium and sodium batteries of high-aspect-ratio, self-organized titania nanotubes, J. Electrochem. Soc. 160 (2013) A1390–A1398.
[30] D. Guan, C. Cai, Y. Wang, Amorphous and crystalline TiO_2 nanotube arrays for enhanced Li-ion intercalation properties, J. Nanosci. Nanotechnol. 11 (2011) 3641–3650.
[31] W.-H. Ryu, D.-H. Nam, Y.-S. Ko, R.-H. Kim, H.-S. Kwon, Electrochemical performance of a smooth and highly ordered TiO2 nanotube electrode for Li-ion batteries, Electrochim. Acta 61 (2012) 19–24.
[32] R. Kirchgeorg, M. Kallert, N. Liu, R. Hahn, M.S. Killian, P. Schmuki, Key factors for an improved lithium ion storage capacity of anodic TiO_2 nanotubes, Electrochim. Acta 198 (2016) 56–65.
[33] L.L. Wang, S.C. Zhang, X.M. Wu, Electrochemical properties of highly ordered TiO_2 nanotube Arrays as an anode material for lithium-ion batteries, Appl. Mech. Mater. 130–134 (2011) 1281–1285.
[34] M. Bratić, D. Jugović, M. Mitrić, N. Cvjetićanin, Insertion of lithium ion in anatase TiO2 nanotube arrays of different morphology, J. Alloys Compd. 712 (2017) 90–96.
[35] A.R. Armstrong, G. Armstrong, J. Canales, R. García, P.G. Bruce, Lithium-ion intercalation into TiO_2-B nanowires, Adv. Mater. 17 (2005) 862–865.
[36] Q. Wang, Z.H. Wen, J.H. Li, A hybrid supercapacitor fabricated with a carbon nanotube cathode and a TiO_2–B nanowire anode, Adv. Funct. Mater. 16 (2006) 2141–2146.
[37] I. Moriguchi, R. Hidaka, H. Yamada, T. Kudo, H. Murakami, N. Nakashima, A mesoporous nanocomposite of TiO_2 and carbon nanotubes as a high-rate Li-intercalation electrode material, Adv. Mater. 18 (2006) 69–73.
[38] Y.-G. Guo, Y.-S. Hu, W. Sigle, J. Maier, Superior electrode performance of nanostructured mesoporous TiO2 (anatase) through efficient hierarchical mixed conducting networks, Adv. Mater. 19 (2007) 2087–2091.
[39] H.T. Fang, M. Liu, D.W. Wang, T. Sun, D.S. Guan, F. Li, J. Zhou, T.K. Sham, H. M. Cheng, Comparison of the rate capability of nanostructured amorphous and anatase TiO_2 for lithium insertion using anodic TiO_2 nanotube arrays, Nanotechnology 20 (2009) 225701.
[40] A. Lamberti, N. Garino, A. Sacco, S. Bianco, A. Chiodoni, C. Gerbaldi, As-grown vertically aligned amorphous TiO_2 nanotube arrays as high-rate Li-based micro-battery anodes with improved long-term performance, Electrochim. Acta 151 (2015) 222–229.
[41] D.-W. Wang, H.-T. Fang, F. Li, Z.-G. Chen, Q.-S. Zhong, G.Q. Lu, H.-M. Cheng, Aligned titania nanotubes as an intercalation anode material for hybrid electrochemical energy storage, Adv. Funct. Mater. 18 (2008) 3787–3793.
[42] Z. Bi, M.P. Paranthaman, P.A. Menchhofer, R.R. Dehoff, C.A. Bridges, M. Chi, B. Guo, X.-G. Sun, S. Dai, Self-organized amorphous TiO_2 nanotube arrays on porous Ti foam for rechargeable lithium and sodium ion batteries, J. Power Sources 222 (2013) 461–466.
[43] H. Choi, H. Park, J.H. Um, W.-S. Yoon, H. Choe, Processing and characterization of titanium dioxide grown on titanium foam for potential use as Li-ion electrode, Appl. Surf. Sci. 411 (2017) 363–367.
[44] J.-H. Kim, K. Zhu, J.Y. Kim, A.J. Frank, Tailoring oriented TiO_2 nanotube morphology for improved Li storage kinetics, Electrochim. Acta 88 (2013) 123–128.
[45] H. Xiong, H. Yildirim, E.V. Shevchenko, V.B. Prakapenka, B. Koo, M.D. Slater, M. Balasubramanian, S.K.R.S. Sankaranarayanan, J.P. Greeley, S. Tepavcevic, N. M. Dimitrijevic, P. Podsiadlo, C.S. Johnson, T. Rajh, Self-improving anode for lithium-ion batteries based on amorphous to cubic phase transition in TiO_2 nanotubes, J. Phys. Chem. C 116 (2012) 3181–3187.
[46] Y. Jiang, C. Hall, N. Song, D. Lau, P. Burr, R. Patterson, D.-W. Wang, Z. Ouyang, A. Lennon, Evidence for fast lithium-ion diffusion and charge transfer reactions in amorphous TiO_x nanotubes: insights for high rate electrochemical energy storage, ACS Appl. Mater. Interfaces 10 (49) (2018) 42513–42523.
[47] D. Steiner, A. Auer, E. Portenkirchner, J. Kunze-Liebhäuser, The role of surface films during lithiation of amorphous and anatase TiO_2 nanotubes, J. Electroanal. Chem. 812 (2018) 166–173.
[48] H. Lindström, S. Södergren, A. Solbrand, H. Rensmo, J. Hjelm, A. Hagfeldt, S.-E. Lindquist, Li+ ion insertion in TiO_2 (anatase). 2. Voltammetry on nanoporous films, J. Phys. Chem. B 101 (1997) 7717–7722.
[49] A.J. Bard, L.R. Faulkner, J. Leddy, C.G. Zoski, Electrochemical Methods: Fundamentals and Applications, Wiley New York1980.

[50] S.-H. Park, R. Tian, J. Coelho, V. Nicolosi, J.N. Coleman, Quantifying the trade-off between absolute capacity and rate performance in battery electrodes, Adv. Energy Mater. 9 (2019) 1901359.
[51] R. Tian, S.-H. Park, P.J. King, G. Cunningham, J. Coelho, V. Nicolosi, J.N. Coleman, Quantifying the factors limiting rate performance in battery electrodes, Nat. Commun. 10 (2019) 1933.
[52] G. Ketteler, S. Yamamoto, H. Bluhm, K. Andersson, D.E. Starr, D.F. Ogletree, H. Ogasawara, A. Nilsson, M. Salmeron, The nature of water nucleation sites on TiO_2(110) surfaces revealed by ambient pressure X-ray photoelectron spectroscopy, J. Phys. Chem. C 111 (2007) 8278–8282.
[53] L. Li, J. Yan, T. Wang, Z.-J. Zhao, J. Zhang, J. Gong, N. Guan, Sub-10 nm rutile titanium dioxide nanoparticles for efficient visible-light-driven photocatalytic hydrogen production, Nat. Commun. 6 (2015) 5881.
[54] A.-Y. Zhang, L.-L. Long, C. Liu, W.-W. Li, H.-Q. Yu, Chemical recycling of the waste anodic electrolyte from the TiO_2 nanotube preparation process to synthesize facet-controlled TiO_2 single crystals as an efficient photocatalyst, Green Chem. 16 (2014) 2745–2753.
[55] S.P. Albu, A. Ghicov, S. Aldabergenova, P. Drechsel, D. LeClere, G.E. Thompson, J. M. Macak, P. Schmuki, formation of double-walled TiO_2 nanotubes and robust anatase membranes, Adv. Mater. 20 (2008) 4135–4139.
[56] D. Regonini, A. Jaroenworaluck, R. Stevens, C.R. Bowen, Effect of heat treatment on the properties and structure of TiO_2 nanotubes: phase composition and chemical composition, Surf. Interface Anal. 42 (2010) 139–144.
[57] D. Yu, X. Zhu, Z. Xu, X. Zhong, Q. Gui, Y. Song, S. Zhang, X. Chen, D. Li, Facile method to enhance the adhesion of TiO_2 nanotube Arrays to Ti substrate, ACS Appl. Mater. Interfaces 6 (2014) 8001–8005.
[58] Y. Zhang, Y. Han, L. Zhang, Interfacial structure of the firmly adhered TiO_2 nanotube films to titanium fabricated by a modified anodization, Thin Solid Films 583 (2015) 151–157.
[59] M. Wagemaker, W.J.H. Borghols, F.M. Mulder, Large impact of particle size on insertion reactions. A Case for Anatase Li_xTiO_2, JACS 129 (2007) 4323–4327.
[60] K. Zhu, Q. Wang, J.-H. Kim, A.A. Pesaran, A.J. Frank, Pseudocapacitive lithium-ion storage in oriented anatase TiO_2 nanotube Arrays, J. Phys. Chem. C 116 (2012) 11895–11899.
[61] A. Auer, E. Portenkirchner, T. Götsch, C. Valero-Vidal, S. Penner, J. Kunze-Liebhäuser, Preferentially oriented TiO_2 nanotubes as anode material for Li-ion batteries: insight into Li-ion storage and lithiation kinetics, ACS Appl. Mater. Interfaces 9 (2017) 36828–36836.
[62] W.J.H. Borghols, D. Lutzenkirchen-Hecht, U. Haake, E.R.H. van Eck, F.M. Mulder, M. Wagemaker, The electronic structure and ionic diffusion of nanoscale $LiTiO_2$ anatase, Phys. Chem. Chem. Phys. 11 (2009) 5742–5748.
[63] S. Ganapathy, S. Basak, A. Lefering, E. Rogers, H.W. Zandbergen, M. Wagemaker, Improving reversible capacities of high-surface lithium insertion materials – the case of amorphous TiO_2, Front. Energy Res. 2 (2014).
[64] J. Han, A. Hirata, J. Du, Y. Ito, T. Fujita, S. Kohara, T. Ina, M. Chen, Intercalation pseudocapacitance of amorphous titanium dioxide@nanoporous graphene for high-rate and large-capacity energy storage, Nano Energy 49 (2018) 354–362.
[65] D. Tie, S. Huang, J. Wang, J. Ma, J. Zhang, Y. Zhao, Hybrid energy storage devices: advanced electrode materials and matching principles, Energy Storage Mater. 21 (2019) 22–40.
[66] Q.L. Wu, J. Li, R.D. Deshpande, N. Subramanian, S.E. Rankin, F. Yang, Y.-T. Cheng, Aligned TiO_2 nanotube Arrays as durable lithium-ion battery negative electrodes, J. Phys. Chem. C 116 (2012) 18669–18677.
[67] S. Huang, D. Tie, M. Wang, B. Wang, P. Jia, Q. Wang, G. Chang, J. Zhang, Y. Zhao, Largely increased lithium storage ability of mangnese oxide through a continuous electronic structure modulation and elevated capacitive contribution, ACS Sustain. Chem. Eng. 7 (2019) 740–747.
[68] G. Wentian, Y. Gleb, Review of nanostructured carbon materials for electrochemical capacitor applications: advantages and limitations of activated carbon, carbide-derived carbon, zeolite-templated carbon, carbon aerogels, carbon nanotubes, onion-like carbon, and graphene, Wiley Interdiscip. Rev.: Energy Environ. 3 (2014) 424–473.
[69] P. Ratajczak, M.E. Suss, F. Kaasik, F. Béguin, Carbon electrodes for capacitive technologies, Energy Storage Mater. 16 (2019) 126–145.
[70] V. Augustyn, P. Simon, B. Dunn, Pseudocapacitive oxide materials for high-rate electrochemical energy storage, Energy Environ. Sci. 7 (2014) 1597–1614.
[71] K. Brezesinski, J. Wang, J. Haetge, C. Reitz, S.O. Steinmueller, S.H. Tolbert, B. M. Smarsly, B. Dunn, T. Brezesinski, Pseudocapacitive contributions to charge storage in highly ordered mesoporous group V transition metal oxides with iso-oriented layered nanocrystalline domains, JACS 132 (2010) 6982–6990.
[72] V. Augustyn, J. Come, M.A. Lowe, J.W. Kim, P.-L. Taberna, S.H. Tolbert, H. D. Abruña, P. Simon, B. Dunn, High-rate electrochemical energy storage through Li + intercalation pseudocapacitance, Nat. Mater. 12 (2013) 518.
[73] Y. Jiang, C. Hall, N. Song, D. Lau, P.A. Burr, R. Patterson, D.-W. Wang, Z. Ouyang, A. Lennon, Evidence for fast lithium-ion diffusion and charge-transfer reactions in amorphous TiOx nanotubes: insights for high-rate electrochemical energy storage, ACS Appl. Mater. Interfaces 10 (2018) 42513–42523.
[74] B. Kang, G. Ceder, Battery materials for ultrafast charging and discharging, Nature 458 (2009) 190.
[75] Y. Sun, K.-P. Yan, Effect of anodization voltage on performance of TiO2 nanotube arrays for hydrogen generation in a two-compartment photoelectrochemical cell, Int. J. Hydrogen Energy 39 (2014) 11368–11375.
[76] S. Bauer, S. Kleber, P. Schmuki, TiO_2 nanotubes: tailoring the geometry in H_3PO_4/HF electrolytes, Electrochem. Commun. 8 (2006) 1321–1325.
[77] J.M. Macak, H. Hildebrand, U. Marten-Jahns, P. Schmuki, Mechanistic aspects and growth of large diameter self-organized TiO2 nanotubes, J. Electroanal. Chem. 621 (2008) 254–266.
[78] J.V. Pasikhani, N. Gilani, A.E. Pirbazari, The effect of the anodization voltage on the geometrical characteristics and photocatalytic activity of TiO2 nanotube arrays, Nano-Structures Nano-Objects 8 (2016) 7–14.
[79] P. Roy, S. Berger, P. Schmuki, TiO_2 nanotubes: synthesis and applications, Angew. Chem. Int. Ed. 50 (2011) 2904–2939.
[80] K. Lee, J. Kim, H. Kim, Y. Lee, Y. Tak, D. Kim, P. Schmuki, Effect of electrolyte conductivity on the formation of a nanotubular TiO_2 photoanode for a dye-sensitized solar cell, J. Kor. Phys. Soc. 54 (2009) 1027.
[81] D. Regonini, C.R. Bowen, A. Jaroenworaluck, R. Stevens, A review of growth mechanism, structure and crystallinity of anodized TiO_2 nanotubes, Mater. Sci. Eng. R Rep. 74 (2013) 377–406.
[82] D. Kim, A. Ghicov, P. Schmuki, TiO2 Nanotube arrays: elimination of disordered top layers ("nanograss") for improved photoconversion efficiency in dye-sensitized solar cells, Electrochem. Commun. 10 (2008) 1835–1838.
[83] K. Indira, U.K. Mudali, T. Nishimura, N. Rajendran, A review on TiO_2 nanotubes: influence of anodization parameters, formation mechanism, properties, corrosion behavior, and biomedical applications, J. Bio Tribo-Corrosion 1 (2015) 28.
[84] K.R. Hebert, J.E. Houser, A model for coupled electrical migration and stress-driven transport in anodic oxide films, J. Electrochem. Soc. 156 (2009) C275–C281.
[85] P. Skeldon, G.E. Thompson, S.J. Garcia-Vergara, L. Iglesias-Rubianes, C.E. Blanco-Pinzon, A tracer study of porous anodic alumina, Electrochem. Solid State Lett. 9 (2006) B47–B51.
[86] P. Acevedo-Peña, L. Lartundo-Rojas, I. González, Effect of water and fluoride content on morphology and barrier layer properties of TiO2 nanotubes grown in ethylene glycol-based electrolytes, J. Solid State Electrochem. 17 (2013) 2939–2947.
[87] M. Madian, M. Klose, T. Jaumann, A. Gebert, S. Oswald, N. Ismail, A. Eychmuller, J. Eckert, L. Giebeler, Anodically fabricated TiO_2-SnO_2 nanotubes and their application in lithium ion batteries, J. Mater. Chem. 4 (2016) 5542–5552.
[88] T. Anwar, L. Wang, L. Tongxiang, X. He, R.U.R. Sagar, K. Shehzad, Effect of aspect ratio of titanium dioxide nanotube arrays on the performance of lithium ion battery, Int. J. Electrochem. Sci. 10 (2015) 6537–6547.
[89] S. Ivanov, L. Cheng, H. Wulfmeier, D. Albrecht, H. Fritze, A. Bund, Electrochemical behavior of anodically obtained titania nanotubes in organic carbonate and ionic liquid based Li ion containing electrolytes, Electrochim, Acta 104 (2013) 228–235.
[90] A. Lamberti, N. Garino, A. Sacco, S. Bianco, D. Manfredi, C. Gerbaldi, Vertically aligned TiO2 nanotube array for high rate Li-based micro-battery anodes with improved durability, Electrochim. Acta 102 (2013) 233–239.
[91] P.P. Prosini, C. Cento, A. Pozio, Electrochemical characterization of titanium oxide nanotubes, Electrochim. Acta 111 (2013) 120–125.
[92] Y. Wang, S. Liu, K. Huang, D. Fang, S. Zhuang, Electrochemical properties of freestanding TiO_2 nanotube membranes annealed in Ar for lithium anode material, J. Solid State Electrochem. 16 (2012) 723–729.
[93] N. Zec, N. Cvjetićanin, M. Bešter-Rogač, M. Vraneš, S. Gadžurić, Electrochemical performance of anatase TiO_2 nanotube Arrays electrode in ionic liquid based electrolyte for lithium ion batteries, J. Electrochem. Soc. 164 (2017) H5100–H5107.